ISSN 0021-3640, JETP Letters, 2014, Vol. 99, No. 2, pp. 99–103. © Pleiades Publishing, Ltd., 2014.
Original Russian Text © A.V. Ushakov, I.V. Karpov, A.A. Lepeshev, M.I. Petrov, L.Yu. Fedorov, 2014, published in Pis'ma v Zhurnal Eksperimental'noi i Teoreticheskoi Fiziki, 2014, Vol. 99, No. 2, pp. 105–109.

Study of Magnetic Flux Pinning in Granular $YBa_2Cu_3O_{7-y}$/nanoZrO_2 Composites

A. V. Ushakov[a, *], I. V. Karpov[a], A. A. Lepeshev[a, b], M. I. Petrov[c], and L. Yu. Fedorov[a]

[a] *Siberian Federal University, Krasnoyarsk, 660074 Russia*

[*] *e-mail: sfu-unesco@mail.ru*

[b] *Krasnoyarsk Scientific Center, Siberian Branch, Russian Academy of Sciences, Krasnoyarsk, 660036 Russia*

[c] *Kirensky Institute of Physics, Siberian Branch, Russian Academy of Sciences, Krasnoyarsk, 660036 Russia*

Received December 23, 2013

In this work, the effect of ZrO_2 nanoparticles prepared in a low-pressure arc discharge plasma on magnetic flux pinning of granular $YBa_2Cu_3O_{7-y}$/nanoZrO_2 composites has been studied. It has been shown that the ZrO_2 nanoparticles do not change the superconducting transition and the microstructure of superconductors. At a temperature of 5 K, the addition of 0.5 and 1 wt % of ZrO_2 nanoparticles may lead to the additional effect of magnetic flux pinning and the increase in the critical current density J_c. The J_c value for composites with 1 wt % is two times larger than that for the reference sample. The fishtail effect is observed for $YBa_2Cu_3O_{7-y}$/nanoZrO_2 composites at the temperatures of 20 and 50 K. The problems associated with the additional effect of magnetic flux pinning of granular $YBa_2Cu_3O_{7-y}$/nanoZrO_2 composites and the appearance of the fishtail effect have been discussed.

DOI: 10.1134/S002136401402009X

High critical current densities J_c are of considerable significance for multiple prospective applications of high-temperature superconductors such as wires for electric energy transmission and magnets [1]. As a rule, the limitation of J_c is connected with two main factors [2]. First, J_c is limited by the thermally activated magnetic flux creep; i.e., it decreases considerably under the action of a magnetic field much less than the critical field $H_c(T)$. This phenomenon is caused by the well-known properties of high-temperature superconductors, e.g., the high anisotropy and small coherence length, which lead to weak magnetic flux pinning. Second, J_c in polycrystalline high-temperature superconductors is limited by the insufficient ordering of crystallites and their chemical inhomogeneity, which leads to weak coupling with low critical current densities. This problem is overcome by different methods of growing the texture such as oxide-powder-in-tube, OPIT [3]. Owing to this technology, the value $J_c > 80$ kA/cm^2 was reached in short multiwire Bi-2223/Ag strips at a temperature of 77 K [4].

In the last years, there appeared many new methods of creating pinning centers and, accordingly, increasing the critical current J_c of high-temperature superconductors. Of the highest interest among them are the following. Amorphous cylindrical tracks with a diameter of about 10 nm and length from 1 to 10 μm were prepared by heavy-ion bombardment of $YBa_2Cu_3O_{7-y}$ single crystals [5]. Tracks in amorphous $Bi_2Sr_2CaCu_2O_8$ were prepared by proton irradiation with the subsequent decay of Bi nuclei [6]. The magnetization hysteresis and critical temperature of $HgBa_2CaCu_2O_6$ were increased by its neutron irradiation [7].

However, the application of these technologies is accompanied by considerable difficulties: serious hindrances in the application of accelerators, radioactive elements, and neutron irradiation.

Obviously, it is necessary to study further the methods of the incorporation of defects or impurities into the superconducting matrix. Apparently, the most realistic approach is the preliminary mixing of nanoparticles and high-temperature superconducting powder and then the performance of the standard technological procedures, i.e., annealing, sintering, and oxygenation (if necessary). The following advantages will be achieved: the possibility of industrial application, the considerable decrease in the anisotropy of magnetic properties, and the considerable increase in the critical current when the contact between the grains is enhanced.

The nanoparticles should meet the following main requirements: first, their size should be comparable with the coherence length of the high-temperature superconductors and, second, they should be stable in a chemically aggressive medium at elevated temperatures. This is necessary for the optimization of superconductivity in the matrix material. In this work, we chose ZrO_2 nanoparticles for studies in the form of inclusions in a polycrystalline superconducting

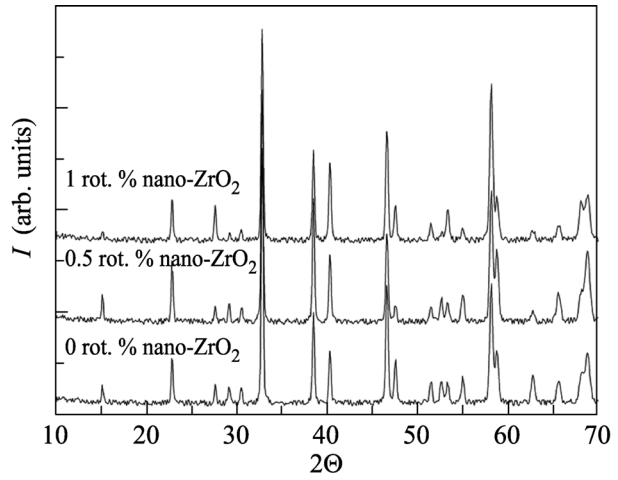

Fig. 1. X-ray diffraction patterns of $YBa_2Cu_3O_{7-y}/ZrO_2$ composites with 0, 0.5, and 1.0 wt % of ZrO_2 nanoparticles.

$YBa_2Cu_3O_{7-y}$ matrix. The melting temperature of ZrO_2 reaches 2400°C. They are chemically stable. The aim of this work is to study the effect of ZrO_2 nanoparticles prepared in a low-pressure arc discharge plasma on the magnetic flux pinning of the granular $YBa_2Cu_3O_{7-y}/nanoZrO_2$ composites.

The powder of the precursor $YBa_2Cu_3O_{7-y}$ was prepared using the conventional solid-phase synthesis. The $YBa_2Cu_3O_{7-y}/nanoZrO_2$ composite was synthesized according to the technique described in detail in [8, 9]. The material was synthesized under the following conditions. Technically pure zirconium was used as the sputtering cathode. Prior to the evaporation, the cathode was heated to a working temperature of 800 K. The purification in the glow discharge was performed at the voltage on the substrate of 1000 V for 1 min. The ion bombardment activation was performed for 1 min at an arc discharge current of 20 A and a voltage on the substrate of 1000 V. The rotation frequency of the mixing device was 8 min^{-1}. The vibration amplitude was 1 mm. The vibration frequency was 50 Hz. The direct deposition of the ZrO_2 nanoparticles on the high-temperature superconducting microgranules was performed at a discharge current of 500 A. The longitudinal magnetic field strength created by the focusing coil of the cathode surface was 6366.2 A/m. To implement the plasma-chemical reaction, a 5% O_2 + 95% He gas mixture was inserted in the chamber using a two-channel regulator of the gas flow rate after the preliminary evacuation to a pressure of 1 mPa. The synthesis was performed at a pressure above 120 Pa. After the deposition of the nanoparticles, the samples were passivated in a pure oxygen atmosphere for a day. The prepared samples of the material contained from 0.1 to 1 wt % of nanoparticles.

The prepared mixture was preliminarily heated to 940°C and kept at this temperature for 30 h. The preliminarily heated powder was ground and then pressed into tablets with a diameter of 1 mm and a thickness of 5 mm at a pressure of 1.2×10^5 N/cm^2. Finally, the granules were sintered at 940°C for 24 h and then cooled to room temperature in an oven in air.

Magnetization was recorded by differential Hall magnetometry with the use of two semiconductor Hall sensors switched opposite to the Hall potential outputs. The first Hall sensor was far from the sample and measured the external magnetic field H. The second sensor was placed on the sample surface and measured the magnetic flux density. As a result of the apparatus subtraction of the Hall potential of the first Hall sensor from the potential of the second Hall sensor, the resultant signal appeared corresponding to the magnetization $M(H)$. According to the Bean formula including the demagnetization factor and the dependence of the critical current on the magnetic field, $J_c(H) = 30M(H)/d$, where M is the width of the magnetic hysteresis loop and d is the average size of the crystallite. We used the value $d = 6$ μm obtained from the electron microscopy results. The hysteresis magnetic loops were measured at 5, 20, and 50 K. The pinning force was calculated using the equation $F_p(B) = J_c(B)B$ [10].

The phase composition of the high-temperature superconducting samples were studied on an XRG-6000 diffractometer using CuK_α radiation. The phase composition and the size of the coherent scattering regions were analyzed using the PCPDFWIN database.

The sample structure was studied by scanning electron microscopy on a JEM-100CX electron microscope with an ASID-4D scanning device at an accelerating voltage of 40 keV.

Figure 1 shows the X-ray diffraction patterns of all $YBa_2Cu_3O_{7-y}/nanoZrO_2$ composites. Peaks related to the admixture of the ZrO_2 phase or other oxides are absent. The characteristic peaks of $YBa_2Cu_3O_{7-y}$ do not shift. The study of the temperature dependence of the magnetic susceptibility showed that the superconducting transition temperature T_c does not change and is 90 K for all samples. No large aggregates of the ZrO_2 nanoparticles were detected using scanning electron microscopy. Thus, the ZrO_2 nanoparticles are homogeneously distributed over the superconducting matrix. The field dependences $F_p(B)$ and J_c of the $YBa_2Cu_3O_{7-y}/nanoZrO_2$ composite are shown in Figs. 2–4.

Figure 2 shows the magnetic field dependences of the calculated critical current density J_c and the pinning force F_p at a temperature of 5 K for all studied composites. It is seen in Fig. 2a that, for all applied magnetic fields, J_c is much higher for composites with 0.5 and 1.0 wt % of ZrO_2 nanoparticles than that for the sample without the addition of ZrO_2 nanoparticles. For the composite with 1.0 wt % of ZrO_2 nano-

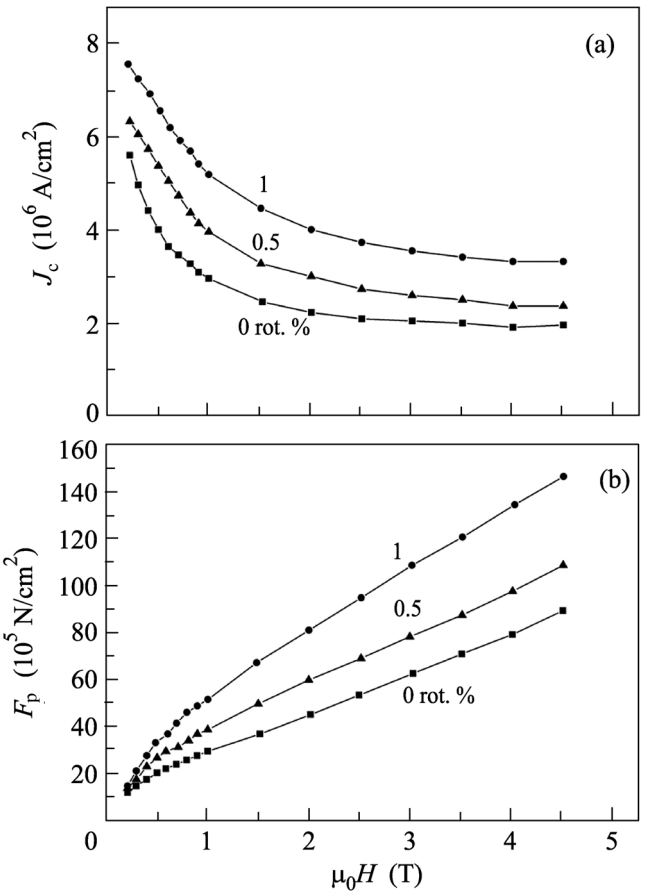

Fig. 2. Magnetic field dependences of (a) J_c and (b) F_p for $YBa_2Cu_3O_{7-y}/ZrO_2$ composites with 0, 0.5, and 1.0 wt % of ZrO_2 nanoparticles at 5 K.

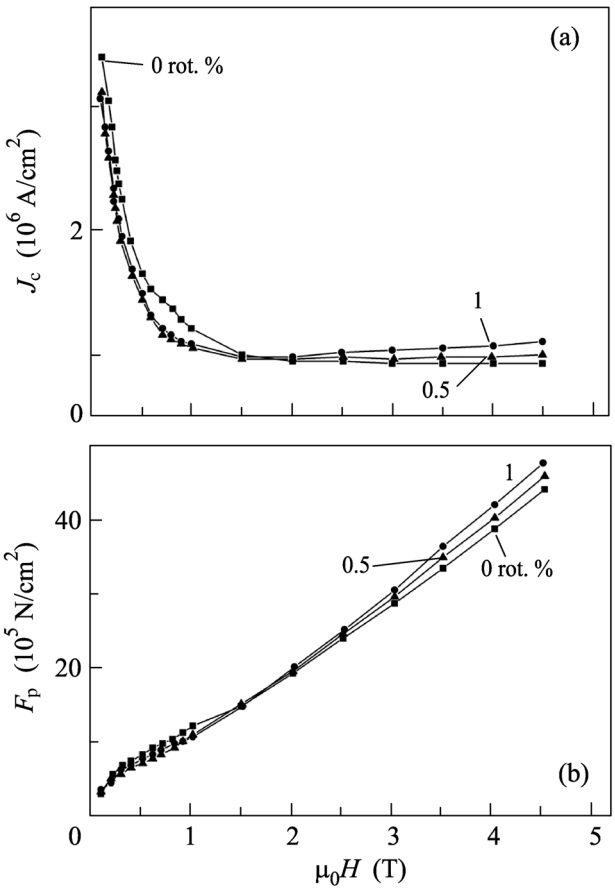

Fig. 3. Magnetic field dependences of (a) J_c and (b) F_p for $YBa_2Cu_3O_{7-y}/ZrO_2$ composites with 0, 0.5, and 1.0 wt % of ZrO_2 nanoparticles at 20 K.

particles, the J_c value is two times higher than that for the samples without nanoparticles. It is seen in Fig. 2b that the pinning force F_p for all composites increases with the applied magnetic field. In the whole range of the applied magnetic field, the pinning force F_p of composites with 0.5 and 0.1 wt % of ZrO_2 nanoparticles is higher than that of the pure sample $YBa_2Cu_3O_{7-y}$. These plots show that the addition of the ZrO_2 nanoparticles leads to the formation of additional effective pinning centers. These centers can increase the pinning force of $YBa_2Cu_3O_{7-y}$ superconductors and improve their critical current densities J_c at a temperature of 5 K.

Figure 3 shows the magnetic field dependences of the calculated critical current density J_c and the pinning force F_p at the temperature of 20 K for all studied composites. It is seen that, for the samples with 0.5 and 1.0 wt % of ZrO_2 nanoparticles at a magnetic field below 1.5 T, J_c and F_p are less than the respective values for samples without the ZrO_2 nanoparticles. However, in the field range from 1.5 to 5 T, the J_c value of the samples with 0.5 and 1.0 wt % of ZrO_2 nanoparticles is comparable with that for the pure sample $YBa_2Cu_3O_{7-y}$. This fact indicates that the ZrO_2 nanoparticles enhance the weak intergranular bonds of $YBa_2Cu_3O_{7-y}$ in the specified magnetic field range. As the magnetic field increases above 2 T, the critical current density for the $YBa_2Cu_3O_{7-y}$/nanoZrO_2 composites with 0, 0.5, and 1.0 wt % of ZrO_2 nanoparticles increases, i.e., the fishtail effect is observed.

Figure 4 shows the magnetic field dependences of the calculated critical current density J_c and the pinning force F_p at a temperature of 50 K for all studied composites. It can be seen that J_c and F_p for the samples with 0.5 and 1.0 wt % of ZrO_2 nanoparticles are less than those for the samples without ZrO_2 nanoparticles at a magnetic field below 0.8 T. This fact means that the additives of ZrO_2 nanoparticles in the specified magnetic field range favor the weakening of the intergranular bonds of the superconductor. However, for a magnetic field in the range from 0.8 to 3 T, J_c of composites is higher than that of the reference sample. For a field above 3 T, J_c of composites is less than that

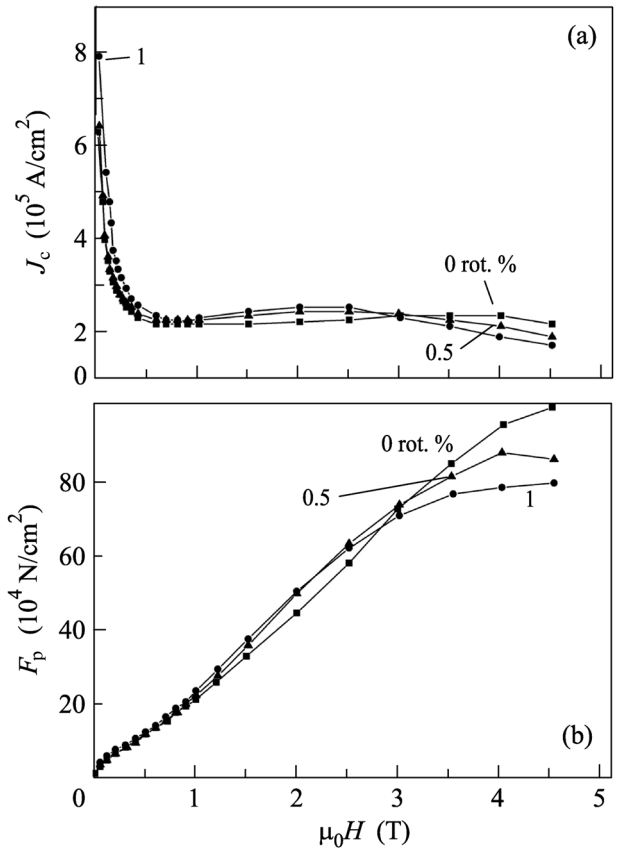

Fig. 4. Magnetic field dependences of (a) J_c and (b) F_p for $YBa_2Cu_3O_{7-y}/ZrO_2$ composites with 0, 0.5, and 1.0 wt % of ZrO_2 nanoparticles at 50 K.

of the reference sample; i.e., the fishtail effect is also observed.

An analogous behavior is observed for the magnetic field dependence of the pinning force. The results obtained show that the addition of the nonsuperconducting ZrO_2 nanoparticles homogeneously dispersed in the matrix in the YBCO superconducting systems can affect magnetic flux pinning and creep. The role of the ZrO_2 nanoparticles in the increase in the critical current density is similar to the role of inclusions of the phase 211 [11]. It assumes that the decreased size of these particles directly conditions the increased pinning. At the same time, rather large particles of the normal (nonsuperconducting) phase 211 naturally decrease the superconducting properties of the sample. Therefore, to optimize the properties of the ceramic, it is necessary to control the concentration and size of the ZrO_2 nanoparticles in the precursor powder used for the preparation of YBCO [12].

No general understanding has been achieved yet concerning the mechanism of the effect of Y211 on pinning in high-temperature superconducting fused textured ceramic materials on the basis of $YBa_2Cu_3O_{7-y}$. In [13], it was assumed that the Y211 particles may act as an effective flux of the pinning centers. In [14], there was an attempt to semiquantitatively theoretically interpret the behavior of $J_c(T, H)$ at high temperatures in high magnetic fields. The authors of [15] considered the defects associated with the interface of the Y211 particles and $YBa_2Cu_3O_{7-y}$ as effective pinning centers, which was confirmed quite successively by many experimental results. An alternative explanation of the increase in the current density J_c may be the transition from the ordered state of the vortex lattice to the disordered state because of the interaction of the lattice with ZrO_2 nanoparticles. It is assumed [16] that the order–disorder transition is implemented if the transverse deformations of the vortex filaments u satisfy the Lindemann criterion: $u = c_L a_0$, where c_L is the Lindemann number, $a_0 = (\Phi_0/B)^{1/2}$ is the intervortex distance, and Φ_0 is the magnetic flux quantum. These deformations lead to the increase in the elastic energy of the order–disorder transition. Therefore, the order–disorder transition is implemented when the increase in the elastic energy $E_e l$ is compensated by the pinning energy E_p. The energy E_p does not depend on the angle at pinning on point defects.

Many studies show that the oxygen vacancies lead to the appearance of the fishtail effects in $YBa_2Cu_3O_{7-y}$ samples [13]. It was established that the oxygen saturation of samples under its controlled isostatic pressure and high temperatures (under the condition of the initial heating to high temperatures in a nitrogen medium) makes it possible to considerably decrease the crack formation in the YBCO ceramics, increase the mechanical characteristics of the material and accelerate the saturation process, and achieve the record high values of the critical current density.

The average size of the ZrO_2 nanoparticles is considerably larger than the coherence length of $YBa_2Cu_3O_{7-y}$ superconductors. Therefore, the statement that the ZrO_2 nanoparticles act as effective pinning centers seems to be incorrect. In addition, the average size of the ZrO_2 nanoparticles is comparable with the penetration depth of the system of YBaCuO superconductors, so that the role of the interphase pinning in $ZrO_2/YBa_2Cu_3O_{7-y}$ systems is limited. In our opinion, ZrO_2 nanoparticles in the $YBa_2Cu_3O_{7-y}$ superconductor are responsible for the pinning expansion. They lead to the distortions of the crystal structure on the interface surface, affect the distribution of the oxygen-deficient regions, and increase the number of microregions with low J_c. In this respect, $ZrO_2/YBa_2Cu_3O_{7-y}$ composites in comparison with pure samples manifest the enhancement of pinning in wide temperature and magnetic field ranges. As a result, they have a higher critical current density.

At a low temperature (in our case, $T = 5$ K), the role of the localized microregions is minimal. For this reason, we did not observe the fishtail effects in

$ZrO_2/YBa_2Cu_3O_{7-y}$ composites with additives of 0, 0.5, and 1.0% of ZrO_2 nanoparticles. At higher temperatures ($T = 20$ and 50 K), the role of the localized microregions is manifested, the additional pinning center flux appears, and the fishtail effect can be observed for all $ZrO_2/YBa_2Cu_3O_{7-y}$ composites.

Thus, ZrO_2 nanoparticles homogeneously dispersed in the matrix of $YBa_2Cu_3O_{7-y}$ superconductors can lead to the existence of additional effective magnetic flux pinning centers. As a result, the critical current density J_c in the $ZrO_2/YBa_2Cu_3O_{7-y}$ composite with 1.0% of ZrO_2 nanoparticles is improved twofold in comparison with that of the pure $YBa_2Cu_3O_{7-y}$ superconductor. At temperatures of 20 and 50 K, the fishtail effect was observed in the magnetic field dependences of the current density and pinning force in all studied $ZrO_2/YBa_2Cu_3O_{7-y}$ composites. ZrO_2 nanoparticles cause the distortions of the crystal structure on the interface surface and affect the distribution of the oxygen-deficient regions. In addition, they are responsible for an increase in the number of microregions with low density J_c.

This work was supported in part by the Ministry of Education and Sciences of the Russian Federation (project no. 7.4484.2011).

REFERENCES

1. S. R. Foltyn, L. Civale, J. L. MacManus-Driscoll, Q. X. Jia, B. Maiorov, H. Wang, and M. Maley, Nature Mater. **6**, 631 (2007).
2. D. Larbalestier, A. Gurevich, D. Feldmann, and A. Polyanskii, Nature **414**, 368 (2001).
3. L. R. Vale, R. H. Ono, and D. A. Rudman, IEEE Trans. Appl. Supercond. **7**, 3193 (1997).
4. C. C. Chin, R. J. Lin, Y. C. Yu, C. W. Wang, E. K. Lin, W. C. Tsai, and T. Y. Tseng, IEEE Trans. Appl. Supercond. **7**, 1403 (1997).
5. A. Goyal, S. Kang, K. J. Leonard, P. M. Martin, A. A. Gapud, M. Varela, M. Paranthaman, A. O. Ijaduola, E. D. Specht, J. R. Thompson, D. K. Christen, S. J. Pennycook, and F. A. List, Supercond. Sci. Tech. **18**, 1533 (2005).
6. D. P. Norton, A. Goyal, J. D. Budai, D. K. Christen, D. M. Kroeger, E. D. Specht, Q. He, B. Saffian, M. Paranthaman, C. E. Klabunde, D. F. Lee, B. C. Sales, and F. A. List, Science **274**, 755 (1996).
7. A. Goyal, D. P. Norton, D. M. Kroeger, D. K. Christen, M. Paranthaman, E. D. Specht, J. D. Budai, Q. He, B. Saffian, F. A. List, D. F. Lee, P. M. Martin, C. E. Klabunde, E. Hatfield, J. Mathis, and C. Park, J. Mater. Res. **12**, 2924 (1997).
8. I. V. Karpov, A. V. Ushakov, L. Yu. Fedorov, and A. A. Lepeshev, Zh. Tekh. Fiz. **84**, 93 (2014).
9. RF Patent No. 2486990.
10. T. Mochida, N. Chikumoto, and M. Murakami, Phys. Rev. B **62**, 1352 (2000).
11. S. Sengupta, D. Shi, Z. Wang, A. C. Biondo, U. Balachandran, and K. C. Goretta, Phys. C **199**, 43 (1992).
12. W. Lo, D. A. Cardwell, S. L. Dung, and R. G. Barter, J. Mater. Res. **11**, 39 (1996).
13. T. A. Prikhna, W. Gawalek, F. Sandiumenge, V. E. Moshchil, V. S. Melnikov, S. N. Dub, T. Habisreuther, A. B. Surzhenko, and P. A. Nagorny, J. Mater. Sci. **35**, 1607 (2000).
14. K. Salama and D. F. Lee, Supercond. Sci. Technol. **7**, 177 (1994).
15. D. F. Lee, V. Selvamanickan, and K. Salama, Phys. C **202**, 83 (1992).
16. D. Ertas and D. R. Neison, Phys. C **272**, 79 (1996).

Translated by L. Mosina